

The effect of anisotropic and isotropic roughness on the convective stability of the rotating disk boundary layer

A. J. Cooper,¹ J. H. Harris,² S. J. Garrett,³ M. Özkan,² and P. J. Thomas²

¹Mathematics Institute, University of Warwick, Coventry CV4 7AL, United Kingdom

²School of Engineering, University of Warwick, Coventry CV4 7AL, United Kingdom

³Department of Engineering, University of Leicester, Leicester LE1 7RH, United Kingdom

(Received 12 March 2014; accepted 29 December 2014; published online 21 January 2015)

A theoretical study investigating the effects of both anisotropic and isotropic surface roughness on the convective stability of the boundary-layer flow over a rotating disk is described. Surface roughness is modelled using a partial-slip approach, which yields steady-flow profiles for the relevant velocity components of the boundary-layer flow which are a departure from the classic von Kármán solution for a smooth disk. These are then subjected to a linear stability analysis to reveal how roughness affects the stability characteristics of the inviscid Type I (or cross-flow) instability and the viscous Type II instability that arise in the rotating disk boundary layer. Stationary modes are studied and both anisotropic (concentric grooves and radial grooves) and isotropic (general) roughness are shown to have a stabilizing effect on the Type I instability. For the viscous Type II instability, it was found that a disk with concentric grooves has a strongly destabilizing effect, whereas a disk with radial grooves or general isotropic roughness has a stabilizing effect on this mode. In order to extract possible underlying physical mechanisms behind the effects of roughness, and in order to reconfirm the results of the linear stability analysis, an integral energy equation for three-dimensional disturbances to the undisturbed three-dimensional boundary-layer flow is used. For anisotropic roughness, the stabilizing effect on the Type I mode is brought about by reductions in energy production in the boundary layer, whilst the destabilizing effect of concentric grooves on the Type II mode results from a reduction in energy dissipation. For isotropic roughness, both modes are stabilized by combinations of reduced energy production and increased dissipation. © 2015 AIP Publishing LLC. [<http://dx.doi.org/10.1063/1.4906091>]

I. INTRODUCTION

Classically it was believed that surface roughness of bodies inevitably increases their skin-friction drag as they move through fluids. However, research more recently has overturned this view.¹⁻³ The practical relevance of this insight is that it opens up the possibility of using suitably designed roughness as a means of developing new drag reduction techniques. There exist two different strategies for achieving this goal. One option is to utilize the effects of roughness in order to reduce the high shear stresses associated with the turbulent boundary layers that are encountered in most technological applications. This approach exploits energetically beneficial interactions between coherent, energy-bearing eddy structures and roughness protrusions to reduce the drag forces generated. The alternative option is to use roughness to delay laminar-turbulent transition in the first place, and thereby utilize the benefits arising from the lower viscous drag forces that are associated with laminar boundary layers. The latter approach is the one focussed on in this study.

The major challenge that remains is to identify what constitutes the *right sort of roughness* for either one of these two approaches, where the aim is to reduce drag in the context of the intended specific technological application and for the particular type of boundary layer encountered. The structure of boundary-layer flows can differ fundamentally, and associated with this are different characteristics of, and implications for, their laminar-turbulent transition process. For instance,

boundary-layer flows can be essentially two dimensional (2D) or fully three dimensional (3D) in nature. The former is the case for the flow over a flat plate whilst the latter type is typically encountered over highly swept wings of aircraft and in many applications involving rotating components such as a rotating disk.⁴⁻⁶

The flow in the boundary layer over a flat plate is 2D in the sense that the undisturbed, steady-state flow has one component of its flow velocity aligned parallel to the plate surface and a second one perpendicular to it. However, in the boundary-layer flow over swept wings of aircraft there exists a third velocity component aligned perpendicular relative to the two components encountered in the flat-plate boundary layer; this third component is the so-called cross-flow velocity. A generic type of boundary layer exhibiting a cross-flow component is the flow over a rotating disk. Here, it is the centrifugally induced radial flow velocity that constitutes the cross-flow component, in addition to an azimuthal component and a component perpendicular to the rotating disk.

Boundary layers with a cross-flow component give rise to a characteristic flow instability—the cross-flow instability—which arises as a consequence of an inflection point in the cross-flow velocity profile. This instability, also referred to as the Type I instability mode, reveals itself in experiments in the form of a series of co-rotating vortices within the transition region⁴⁻¹² with classic, frequently cited photographs.^{13,14} For practical and theoretical reasons, the rotating-disk boundary layer has served as the paradigm for studying boundary layers with a cross-flow component for over six decades^{4,6-8,13,15-17} and is thus chosen for this study.

Early work on the 3D rotating-disk flow was mostly limited to flow transition over smooth disks. Experimental studies were focused almost exclusively on disks designed to test theoretical predictions which had been obtained for hypothetical, idealized flow conditions rarely present in real-world engineering environments. Since the late 1990s studies on non-smooth disks started appearing in the literature and have made substantial contributions to advancing our understanding of the effects of surface disturbances on the laminar-turbulent transition of 3D boundary layers with a cross-flow component. However, the existing studies focussed almost exclusively on the effects of a small number of roughness elements arranged to form certain roughness patterns, the goal being to excite particular disturbance modes to test their characteristics for the development of specific control mechanisms.^{9,10,18-20} Work with more general roughness was briefly considered by Zoueshtiagh *et al.*²¹ for a rotating disk and, in more depth, by Watanabe *et al.*²² Zoueshtiagh *et al.*²¹ documented a short set of experimental data for velocity profiles over quartz-grain roughened disks and these will be revisited here after the presentation of the current results. Watanabe *et al.*²² studied uniformly distributed roughness on a rotating cone. Their study revealed the very interesting result that, with a roughness level that was considered as modest in their particular experiments, the number of the vortices associated with the cross-flow instability decreased from initially 32 for a smooth cone to 26 for the rough cone. This raises questions as to whether higher roughness levels would have reduced the number of spiral vortices further and whether transition can possibly bypass the spiral-vortex route entirely above a certain critical roughness level. This would indicate roughness promoting an entirely different transition mechanism associated with different energetical implications.

Our intention is to begin to study the effects of general surface roughness and specifically the type and level of roughness. The goal is to establish what effect roughness has on the characteristic instability modes that are known to exist in the three-dimensional rotating disk boundary-layer. The study is focussed on stationary disturbances, as these are known to be naturally excited by roughnesses on the disk surface, but non-stationary disturbances and the absolute instability identified by Lingwood¹⁷ are also briefly considered.

Two distinct theoretical models for the steady boundary-layer flow over rough rotating disks exist in the literature. They were developed by Miklavčič and Wang²³ and Yoon *et al.*²⁴ and are henceforth referred to as the MW and YHP models, respectively. Both models show how successively increasing roughness levels lead to deviations from the classic similarity solution for the smooth disk due to von Kármán.²⁵ The YHP approach models roughness by imposing a particular surface distribution as a function of radial position and assumes a rotational symmetry. The YHP model, however, is only capable of modelling the roughness in the radial direction, i.e., a particular case of anisotropic roughness. The MW approach models roughness empirically by replacing the usual no-slip boundary conditions with *partial slip* conditions at the disk surface. The MW model is therefore capable

of modelling independent levels of roughness in the radial and azimuthal directions by separately modifying the boundary conditions in these directions. The case of uniform levels of roughness in every direction over a surface is typically referred to as *isotropic roughness*, and non-uniform levels of roughness as *anisotropic roughness*. The MW model is clearly capable of modelling both anisotropic and isotropic roughness and is the one used in this study. As part of this study we have, however, conducted comparisons between results based on the MW model discussed here and corresponding results produced using the YHP model. While these comparisons are not included, it is emphasized that we found very close qualitative agreement between the results for both models. This close agreement gives confidence in our results based on the partial-slip MW model.

The paper proceeds as follows. In Sec. II, the calculations for steady boundary-layer flows over rotating disks with anisotropic and isotropic surface roughness are summarized. The convective stability properties of the two sets of resulting steady flows are investigated in Sec. III, where neutral curves, critical Reynolds numbers, growth rates, and amplitude ratios for different levels of roughness are presented. In Sec. IV, an analysis of the energy balance within the boundary layers is described, in order to extract possible underlying physical mechanisms behind the effects of roughness on the stability of the flows. Conclusions are then drawn in Sec. VI.

II. THE STEADY FLOW

In this section, the MW model is used without modification and is summarized below for clarity; full details are available in Miklavčič and Wang.²³

The disk is considered to be infinite in diameter and rotating about its axis of symmetry at a constant rotation rate Ω . It is natural to consider this geometry in a cylindrical polar coordinate system (r^*, θ, z^*) in which the governing Navier–Stokes equations are well known. All dimensional quantities are scaled on a characteristic length-scale given by the boundary-layer thickness scale, $\delta^* = \sqrt{\nu/\Omega}$, and a velocity scale given by $r_e^* \Omega$, where r_e^* is a fixed radial position for the stability analysis and ν is the kinematic viscosity. This leads to the Reynolds number $Re = r_e^* \Omega \delta^* / \nu$ and non-dimensional coordinate system (r, θ, z) . The steady flow field is obtained from the exact similarity solution of the Navier–Stokes equations due to von Kármán. All analysis is carried out in the rotating frame and the mean velocity field is written in the form

$$[u^*, v^*, w^*] = [r^* \Omega F(z), r^* \Omega G(z), (\nu \Omega)^{1/2} H(z)],$$

where u^* is the mean radial velocity, v^* the mean azimuthal velocity and w^* the mean axial velocity.

The MW approach assumes that roughness can be modelled by a modification of the no-slip conditions at the disk surface. In particular, the model assumes *partial slip* at the disk surface but is otherwise identical to the smooth disk formulation. The modified wall boundary conditions are expressed as

$$F(0) = \lambda F'(0), \quad (1)$$

$$G(0) = \eta G'(0), \quad (2)$$

where primes denote differentiation with respect to z , and the two parameters η and λ give empirical measures of the roughness in the radial and azimuthal directions, respectively. These boundary conditions reduce to the no-slip boundary conditions for a smooth disk when $\lambda = \eta = 0$. Anisotropic roughness corresponds to the case $\eta > 0, \lambda = 0$ (concentric grooves) or $\eta = 0, \lambda > 0$ (radial grooves), and for isotropic roughness $\lambda = \eta > 0$.

Figures 1, 2, and 3 show the computed flow fields for these three cases at various roughness levels. Our numerical code for the steady flow has been validated against existing results for rotating disk flow with roughness. In particular, our numerical values agree exactly with those appearing in Table 1 of Miklavčič and Wang.²³

For the case of anisotropic roughness with concentric grooves, increasing η results in a slight thickening of the boundary layer and a reduction in the radial jet, as evident in Figure 1(a). Figure 2(a) shows a reduction in the wall value for the azimuthal profile as roughness is increased (a direct result of the partial-slip condition) and Figure 3(a) for the axial velocity profile shows that entrainment of fluid into the boundary layer is reduced as the anisotropic roughness parameter η is

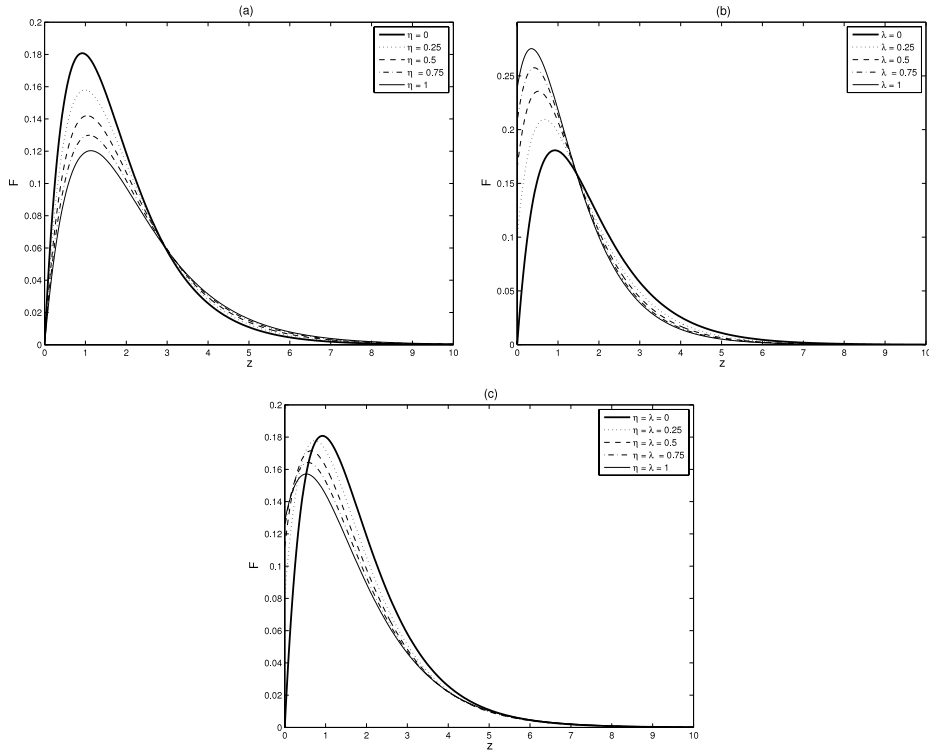


FIG. 1. Steady flow profiles, radial velocity F . (a) Anisotropic roughness—concentric grooves, (b) anisotropic roughness—radial grooves, and (c) isotropic roughness.

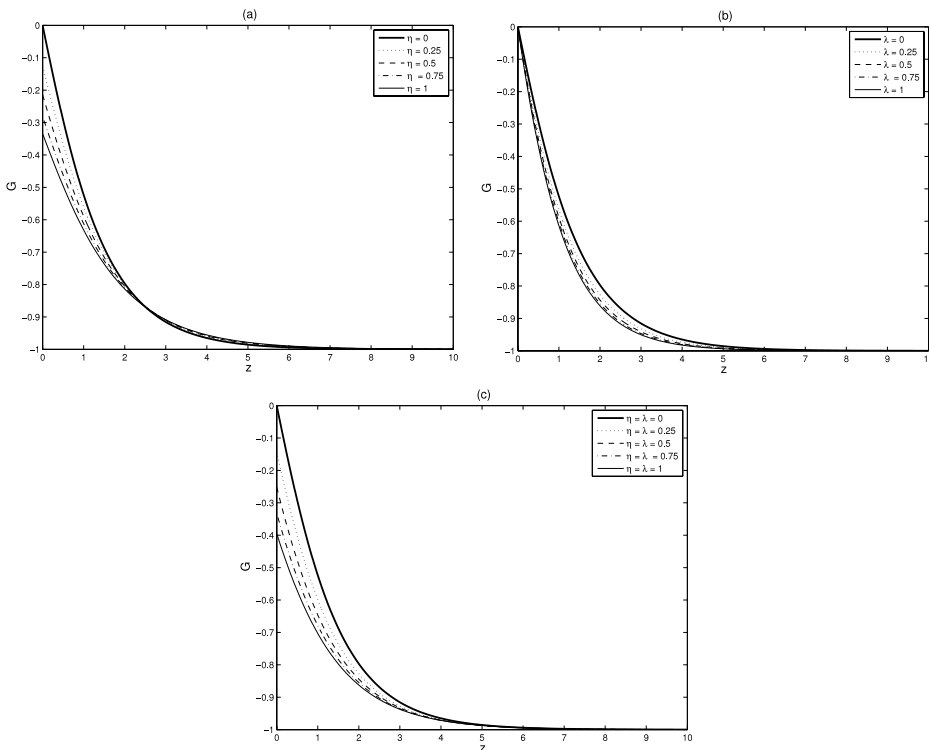


FIG. 2. Steady flow profiles, azimuthal velocity G . (a) Anisotropic roughness—concentric grooves, (b) anisotropic roughness—radial grooves, and (c) isotropic roughness.

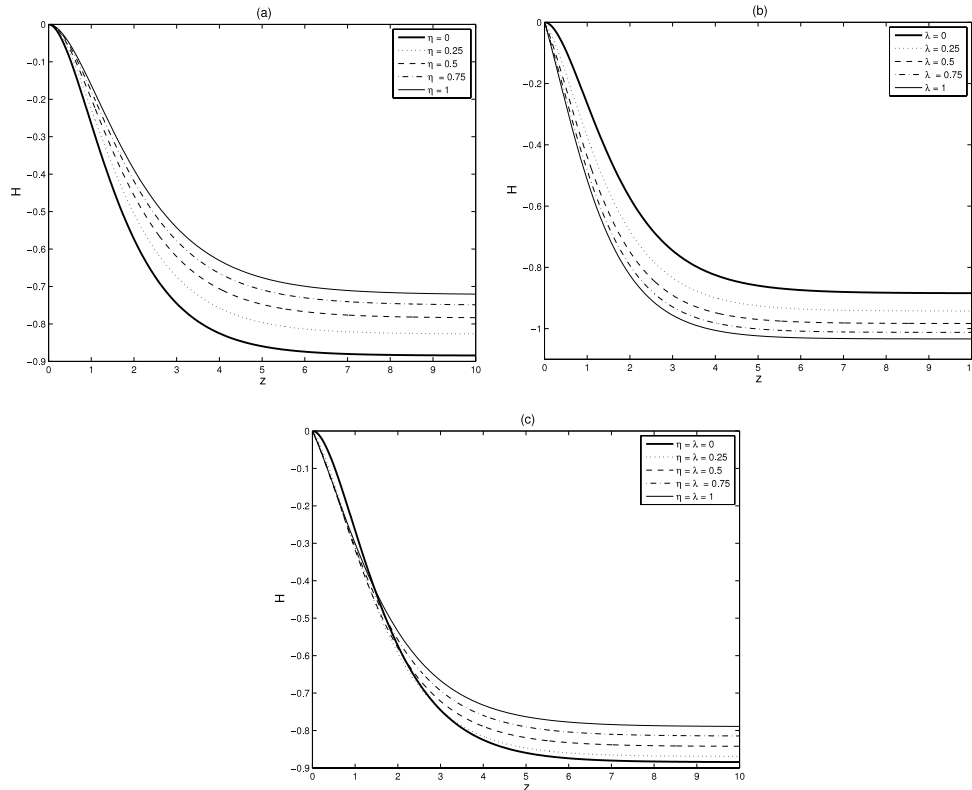


FIG. 3. Steady flow profiles, axial velocity H . (a) Anisotropic roughness—concentric grooves, (b) anisotropic roughness—radial grooves, and (c) isotropic roughness.

increased. In contrast, for the case of radial grooves, there is a slight thinning of the boundary layer and an increase in the radial jet, as seen in Figure 1(b). The partial-slip condition now influences the value of the radial velocity at the wall and consequently increased roughness forces the maximum in the radial velocity closer to the boundary. Radial grooves have little effect on the mean azimuthal velocity as seen in Figure 2(b), but increase the entrainment of fluid into the boundary layer, as shown in Figure 3(b).

For the isotropic case, the effects seen for concentric and radial grooves are combined. Figure 1(c) shows that there is little change to the thickness of the boundary layer but that the maximum radial velocity is reduced and moves towards the disk as a result of increasingly non-zero values for the wall radial velocity. Figure 2(c) shows similar results to the anisotropic concentric-groove case in that the wall azimuthal velocity value decreases with surface roughness. The profiles for the axial velocity in the case of isotropic roughness in Figure 3(c) show that overall there is less fluid entrainment into the boundary layer compared to the smooth disk.

III. CONVECTIVE INSTABILITY

The resulting steady flows are directly related to the von Kármán flow, and, importantly, previous stability analyses for the rotating-disk flow^{17,26,27} are directly applicable to this current study. Full details of the governing perturbation equations and the codes used can be found in those references; here, it is sufficient to understand that a normal-mode analysis is conducted with perturbations of the form

$$(\hat{u}, \hat{v}, \hat{w}, \hat{p}) = (u(z), v(z), w(z), p(z))e^{i(\alpha r + \beta Re\theta - \gamma t)}. \quad (3)$$

The wavenumber in the radial direction, $\alpha = \alpha_r + i\alpha_i$, is complex, as required by the spatial convective analysis to be conducted; the frequency, γ , and circumferential wavenumber, β , are real. It

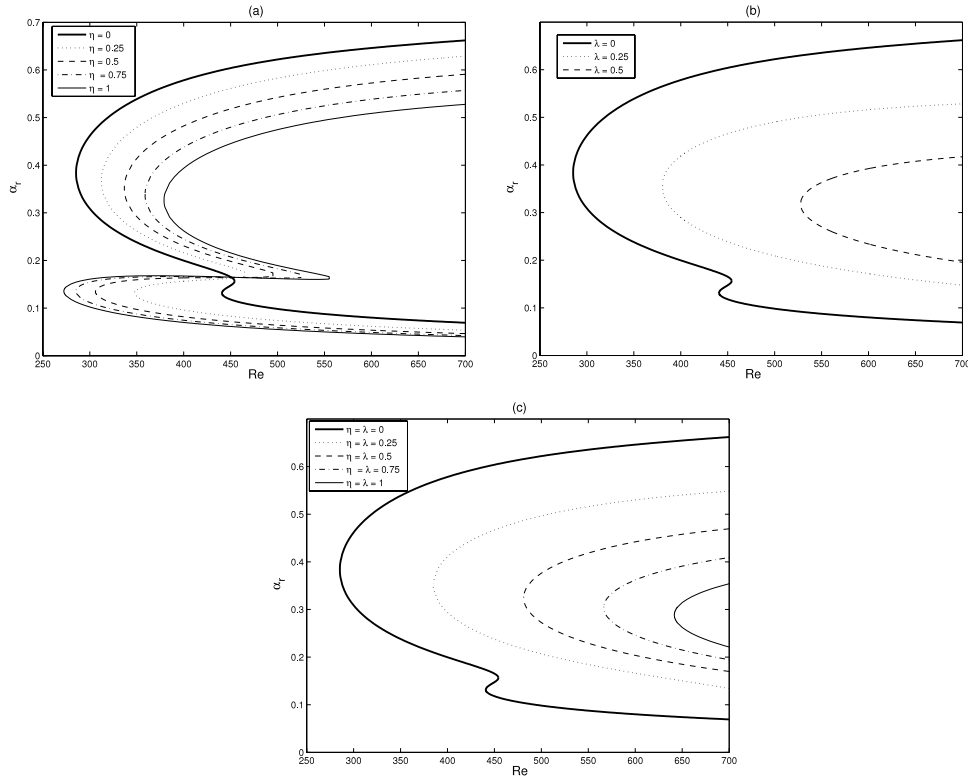


FIG. 4. The radial wavenumber, α_r , as a function of Reynolds number, Re , along the neutral curves. (a) Anisotropic roughness—concentric grooves, (b) anisotropic roughness—radial grooves, and (c) isotropic roughness.

is assumed that β is $O(1)$. The integer number of complete cycles of the disturbance around the azimuth is $n = \beta Re$ and this is identified with the number of spiral vortices around the disk surface. Furthermore, the orientation angle of the vortices with respect to a circle centred on the axis of rotation is $\epsilon = \arctan(\beta/\alpha)$. The quantities n and ϵ can be compared directly to experimental observations. In what follows we are concerned with stationary vortices that rotate with the rough surface and so set $\gamma = 0$. The dispersion relation $D(\alpha, \beta; Re, [\lambda, \eta]) = 0$ is solved with the aim of studying the occurrence of convective instabilities for various values of the roughness parameters λ and η .

As with existing analyses of smooth rotating disks and other related geometries in the literature, two modes are found to determine the convective instability properties of the disturbance modes over rough rotating disks. The Type I mode, appearing as the upper lobe in $\alpha_r - Re$ neutral curves, is known to arise from the inflectional nature of the steady-flow profiles, and the Type II mode, appearing as the lower lobe, is known to arise from streamline curvature and Coriolis effects. Figures 4 and 5 show the neutral curves obtained from concentric and radially grooved disks and for a disk with isotropic roughness in the $\alpha_r - Re$ and $n - Re$ planes, respectively.

The effect of increasing anisotropic roughness in a concentrically grooved disk is to diminish the Type I lobe (both in terms of critical Re and width) whereas it has an increasingly destabilizing effect on the Type II mode, evident through the enhanced region of instability and lowering of the critical Re number as shown in Figures 4(a) and 5(a). In contrast, Figures 4(b) and 5(b) show that radial grooves produce a strongly stabilizing effect on both the Type I and Type II modes, with the Type II lobe vanishing completely for relatively modest levels of roughness. The effect on the Type I mode is also much stronger, with marked reductions in the width of the unstable region and large increases in critical Re compared to the concentric grooves case. For isotropic roughness, the effect on the Type I mode is more strongly stabilising than the case of concentric grooves but not as strong as for radial grooves. The Type II mode is stabilised in the same way as seen for the radially grooved disk. In terms of the number of vortices (see Fig. 5), a concentrically grooved disk tends to lower the

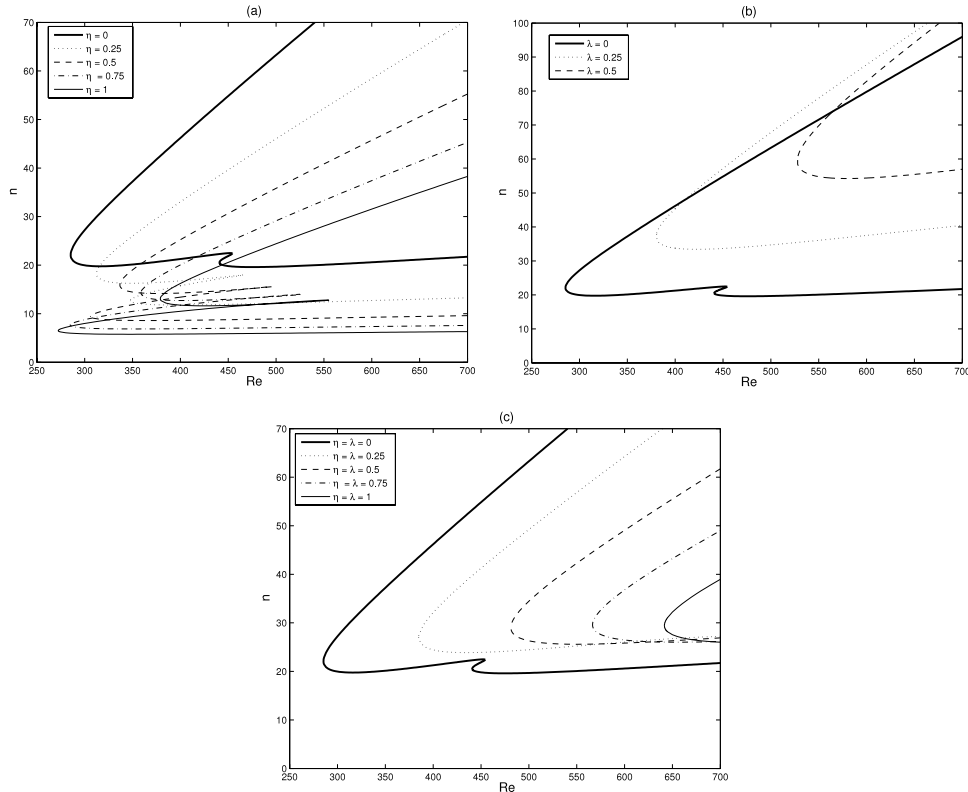


FIG. 5. The number of vortices, n , as a function of Reynolds number, Re , along the neutral curves. (a) Anisotropic roughness—concentric grooves, (b) anisotropic roughness—radial grooves, and (c) isotropic roughness.

number of vortices whilst a radially grooved disk leads to an increase in the number of vortices. For isotropic roughness, there is a slight variation in the number of vortices along the lower branch of the neutral curve, and a lowering of the number of vortices along the upper branch as the roughness is increased. Again this seems to be a tradeoff between the combined effects of azimuthal and radial roughness.

Critical parameters for the onset of the Type I and Type II modes are given in Table I.

It is noted that the behaviour of the Type II mode under anisotropic roughness with concentric grooves is identified as being similar to the effect of wall compliance on this mode,²⁷ where the disk boundary was comprised of a single layer of viscoelastic material free to move under the influence of disturbances in the boundary layer. For certain levels of wall compliance, the Type II lobe of the neutral curve was augmented and the critical Re reduced significantly, in exactly the same way as exhibited in this study.

As well as considering the extent of instability, as indicated by neutral curves, it is also important to consider the effect of roughness on the growth rates within the unstable region. Figure 6 shows the corresponding growth rates at $Re = 400$ for both the Type I and Type II modes under the influence of anisotropic roughness and isotropic roughness. This emphasises the stabilizing effect of anisotropic roughness with concentric grooves on the Type I mode and its destabilizing effect on the Type II mode.

Of particular interest is the most rapidly growing mode, which would be the most likely to dominate and be detected in experiments. The results show a number of key points. In the case of disk with concentric grooves (Fig. 6(a)), it can be seen that for both modes the point of maximum amplification shifts to lower values of n , suggesting a reduction in the number of vortices over the disk. For sufficiently high levels of roughness, the Type II growth rate exceeds the Type I growth rate. For both radial grooves and isotropic roughness (Figs. 6(b) and 6(c)), there is a much stronger stabilizing effect on the Type I mode in terms of growth rate reduction. The effect of radial grooves

TABLE I. Critical values of measurable parameters at the onset of instability under both models. Type I and (Type II). Bold text indicates the most dangerous mode in terms of critical Reynolds number.

Anisotropic roughness—concentric grooves			
Parameter	Re	n	ϵ
$\eta = 0$	285.4 (440.9)	22.1 (20.6)	11.4 (19.5)
$\eta = 0.25$	312.3 (347.5)	18.3 (12.7)	9.1 (15.5)
$\eta = 0.5$	336.8 (306.0)	16.1 (9.4)	7.6 (12.9)
$\eta = 0.75$	358.9 (284.7)	14.4 (7.6)	6.7 (11.3)
$\eta = 1.0$	379.1 (272.4)	13.2 (6.5)	6.0 (10.0)
Anisotropic roughness—radial grooves			
Parameter	Re	n	ϵ
$\lambda = 0$	285.4 (440.9)	22.1 (20.6)	11.4 (19.5)
$\lambda = 0.25$	380.1 (...)	37.0 (...)	15.4 (...)
$\lambda = 0.5$	527.5 (...)	59.4 (...)	19.5 (...)
$\lambda = 0.75$	722.6 (...)	89.4 (...)	23.4 (...)
Isotropic roughness			
Parameter	Re	n	ϵ
$\lambda = \eta = 0$	285.4 (440.9)	22.1 (20.6)	11.4 (19.5)
$\lambda = \eta = 0.25$	384.8 (...)	27.2 (...)	11.2 (...)
$\lambda = \eta = 0.5$	481.2 (...)	29.2 (...)	10.5 (...)
$\lambda = \eta = 0.75$	566.5 (...)	29.7 (...)	9.7 (...)
$\lambda = \eta = 1.0$	641.6 (...)	29.7 (...)	9.0 (...)

is shown to increase the value of n , but for isotropic roughness the overall effect is still to reduce the number of vortices. For radial grooves and isotropic roughness, the growth of the Type II mode is suppressed. These observations raise the possibility that anisotropic vs. isotropic roughness could allow for a potential means of studying the Type II mode experimentally, whereas isotropic roughness would be a stronger candidate to exploit in terms of transition delay.

IV. ENERGY ANALYSIS

Following the work of Cooper and Carpenter,²⁷ an integral energy equation for three-dimensional disturbances ($\hat{u}, \hat{v}, \hat{w}, \hat{p}$) to the undisturbed three-dimensional boundary-layer flow (U, V, W) is derived in order to extract possible underlying physical mechanisms behind the effects of roughness on the stability of rotating disk boundary-layer flow. The energy balance indicates the relative influences of the various energy transfer mechanisms affecting the destabilization of fluid disturbances. This energy equation is obtained by multiplying the linearized momentum equations by \hat{u} , \hat{v} , and \hat{w} , respectively. Summation of the combined equations gives rise to an equation for the kinetic energy of the disturbances as follows:

$$\begin{aligned}
 \left\{ \frac{\partial}{\partial t} + U \frac{\partial}{\partial r} + \frac{V}{r} \frac{\partial}{\partial \theta} + W \frac{\partial}{\partial z} + \frac{\partial}{\partial t} \right\} K = & -\hat{u}\hat{w} \frac{\partial U}{\partial z} - \hat{v}\hat{w} \frac{\partial V}{\partial z} - \hat{w}^2 \frac{\partial W}{\partial z} - \hat{u}^2 \frac{\partial U}{\partial r} - \frac{U\hat{v}^2}{r} \\
 & - \left[\frac{\partial}{\partial r} (\hat{u}\hat{p}) + \frac{1}{r} \frac{\partial}{\partial \theta} (\hat{v}\hat{p}) + \frac{\partial}{\partial z} (\hat{w}\hat{p}) + \frac{\hat{u}\hat{p}}{r} \right] \\
 & + \left[\frac{\partial}{\partial x_i} (\hat{u}_j \sigma_{ij}) - \sigma_{ij} \frac{\partial \hat{u}_j}{\partial x_i} \right], \quad (4)
 \end{aligned}$$

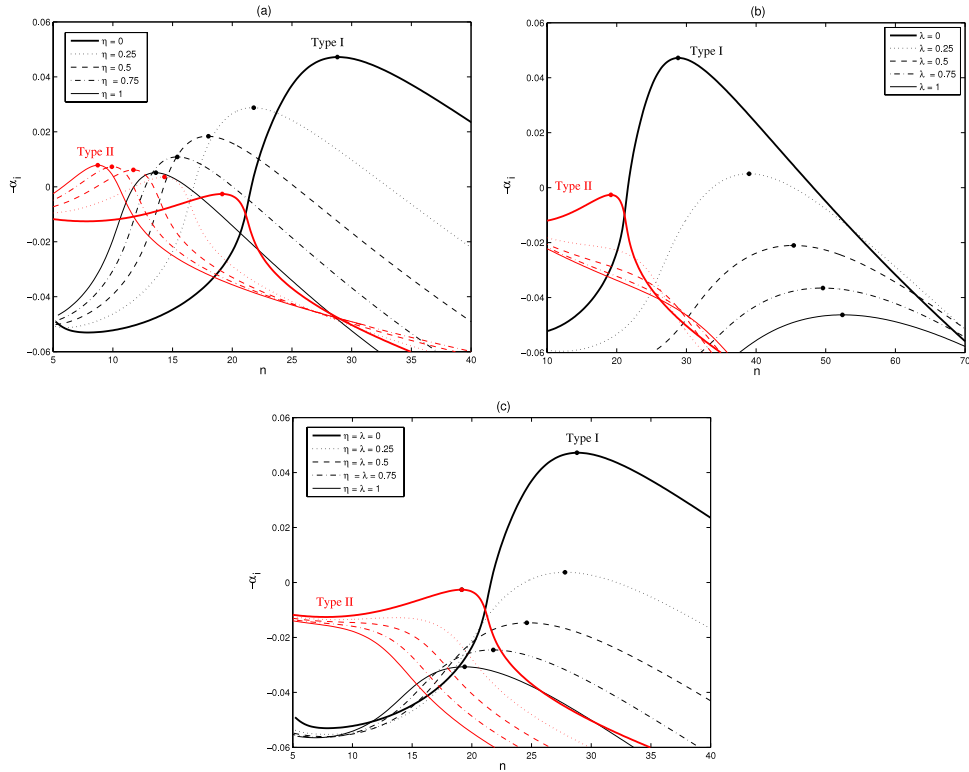


FIG. 6. Growth rate curves at $Re = 400$ as a function of n . (a) Anisotropic roughness—concentric grooves, (b) anisotropic roughness—radial grooves, and (c) isotropic roughness. Black lines denote Type I instability and red lines Type II instability. Dots indicate locations of maximum growth.

where $K = \frac{1}{2}(\hat{u}^2 + \hat{v}^2 + \hat{w}^2)$ and σ_{ij} are the viscous stress terms,

$$\sigma_{ij} = \frac{1}{Re} \left(\frac{\partial \hat{u}_i}{\partial x_j} - \frac{\partial \hat{u}_j}{\partial x_i} \right).$$

Repeated suffices in (4) indicate summation from 1 to 3. Note that $O(1/r)$ viscous terms have been omitted, consistent with neglect of $O(1/Re^2)$ terms in the governing stability equations.

If the perturbations are averaged over a single time period and azimuthal mode, followed by integration across the boundary layer, t and θ derivatives are removed to leave

$$\begin{aligned} & \int_0^\infty \left[\underbrace{U \frac{\partial \bar{K}}{\partial r}}_a + \underbrace{\frac{\partial(\hat{u}\hat{p})}{\partial r}}_b - \underbrace{\frac{\partial}{\partial r}(\hat{u}\sigma_{11} + \hat{v}\sigma_{12} + \hat{w}\sigma_{13})}_c \right] dz \\ & = \int_0^\infty \left[\underbrace{\left(-\hat{u}\hat{w} \frac{\partial U}{\partial z} \right) + \left(-\hat{v}\hat{w} \frac{\partial V}{\partial z} \right) + \left(-\hat{w}^2 \frac{\partial W}{\partial z} \right)}_I dz \right. \\ & \quad - \underbrace{\int_0^\infty \left(\sigma_{ij} \frac{\partial \hat{u}_j}{\partial x_i} \right) dz}_II - \underbrace{\int_0^\infty \left(\frac{\hat{u}\hat{p}}{r} \right) dz}_III + \underbrace{(\hat{w}\hat{p})_w - [\hat{u}\sigma_{31} + \hat{v}\sigma_{32} + \hat{w}\sigma_{33}]_w}_IV \\ & \quad \left. - \underbrace{\int_0^\infty \frac{\partial \bar{K}}{\partial z} W dz - \int_0^\infty \hat{u}^2 \frac{\partial U}{\partial r} dz - \int_0^\infty \frac{\hat{v}^2 U}{r} dz}_V \right] dz, \end{aligned} \tag{5}$$

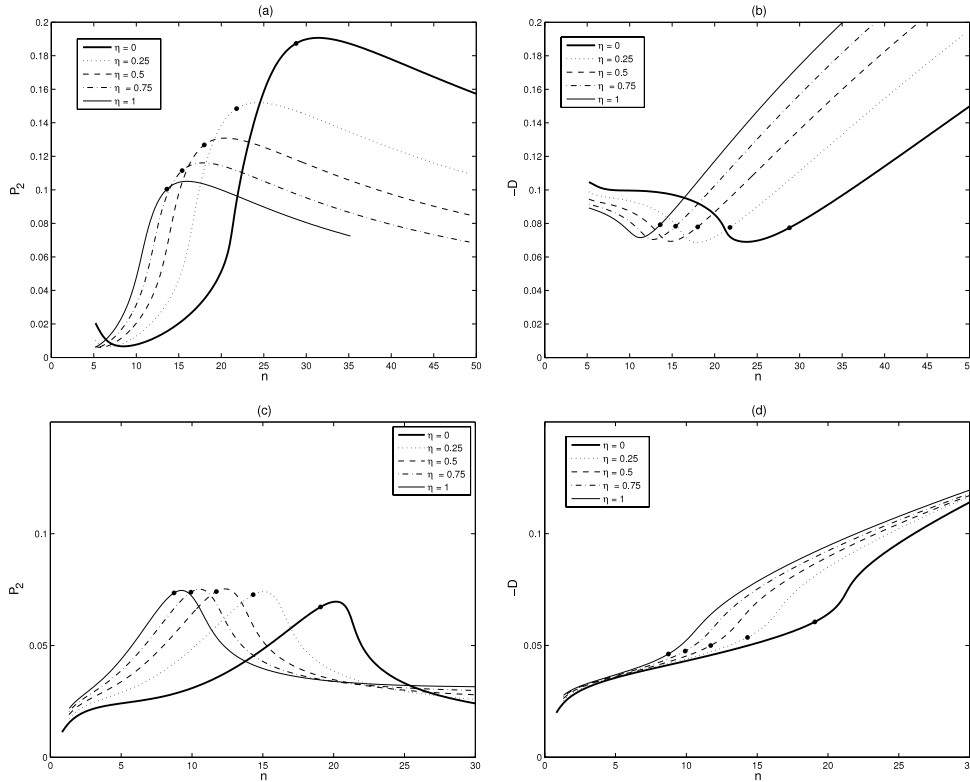


FIG. 7. Energy balance at $Re = 400$ for anisotropic roughness—concentric grooves. (a) Variation in Type I energy production term P_2 with n , (b) variation in Type I viscous dissipation $-D$ with n , (c) variation in Type II energy production term P_2 with n , and (d) variation in Type II viscous dissipation $-D$ with n . Dots correspond to the locations of maximum amplification in Figure 6.

where overbars denote a period-averaged quantity, i.e., $\overline{\hat{u}\hat{v}} = \hat{u}\hat{v}^* + \hat{u}^*\hat{v}$ (* indicates the complex conjugate) and w subscripts denote quantities evaluated at the wall. Terms on the left-hand side can be interpreted physically as (a) the average kinetic energy convected by the radial mean flow, (b) the work done by the perturbation pressure, and (c) the work done by viscous stresses across some internal boundary in the fluid. On the right-hand side there is (I) the Reynolds stress energy production term, (II) the viscous dissipation energy removal term, (III) pressure work terms, (IV) contributions from work done on the wall by viscous stresses, and (V) terms arising from streamline curvature effects and the three-dimensionality of the mean flow.

The energy equation is then normalized by the integrated mechanical energy flux to give

$$-2\alpha_i = \underbrace{(P_1 + P_2 + P_3)}_I + \underbrace{D}_{II} + \underbrace{(PW_1 + PW_2)}_{III} + \underbrace{(S_1 + S_2 + S_3)}_{IV} + \underbrace{(G_1 + G_2 + G_3)}_V. \quad (6)$$

The energy balance can be carried out for any eigenmode. Terms in (6) which are positive contribute to energy production and those which are negative remove energy from the system. A mode is amplified ($\alpha_i < 0$) when energy production outweighs the energy dissipation in the system.

By calculating all terms in the energy equation (6) it is possible to identify where the effects of roughness are the greatest. Given the boundary conditions, some terms in the energy equation are identically zero (PW_2, S_1, S_2, S_3). The main contributors are found to be energy production by the Reynolds stress (P_2) and conventional viscous dissipation (D). Terms P_1, P_3, PW_1 , and G_2 are found to be negligible and the geometric terms G_1 and G_3 remove energy from the system and are relatively larger in the Type II case. The results of the energy balance also reconfirm the results of the linear stability analysis.

The energy balance calculation is carried out across a range of n values at $Re = 400$ and correspond to the growth rate results in Figure 6. Results for various levels of roughness are compared

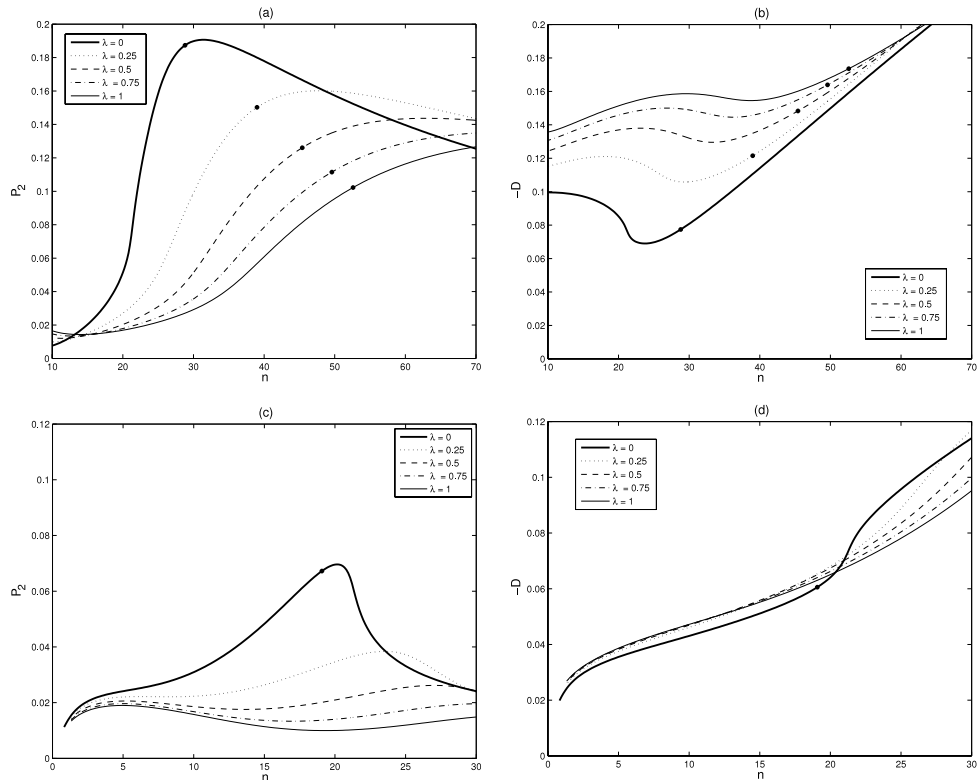


FIG. 8. Energy balance at $Re = 400$ for anisotropic roughness—radial grooves. (a) Variation in Type I energy production term P_2 with n , (b) variation in Type I viscous dissipation $-D$ with n , (c) variation in Type II energy production term P_2 with n , and (d) variation in Type II viscous dissipation $-D$ with n . Dots correspond to the locations of maximum amplification in Figure 6.

to a smooth disk in Figures 7, 8, and 9. For anisotropic roughness with concentric grooves, the major stabilizing effect on the Type I mode is shown to come from a reduction in energy production by Reynolds stresses in the boundary layer. At points of maximum amplification, the viscous dissipation is largely invariant in this case (Figs. 7(a) and 7(b)). Conversely, the major destabilizing effect on the Type II mode comes from a decrease in viscous dissipation at points of maximum amplification, with the energy production term P_2 largely invariant at these points (Figs. 7(c) and 7(d)).

The corresponding results for a radially grooved disk and a disk with isotropic roughness are shown in Figures 8 and 9. These reveal that the Type I mode is stabilized in both of these cases through the action of reduced energy production and increased dissipation. The action of the isotropic roughness parameter λ on the Type II mode in both of these cases is to bring about a reduction in energy production resulting in a stabilizing effect.

The form of the eigenfunctions (or disturbance velocity profiles) provides some explanation for the above trends. The dominant eigenfunction is the azimuthal perturbation velocity, v , which contributes to the dominant energy production term P_2 . Figure 10 shows the magnitude of the v -profile for a concentrically grooved disk. In the case of the Type I mode, the general form of the disturbance profile is preserved as roughness is increased, with the profile being merely translated slightly further into the boundary layer. The dramatic reduction in P_2 in this case results from a strong reduction in the amplitude of the normal velocity, w , as roughness increases. Corresponding results for the Type II mode indicate that the effects of roughness are seen through the eigenfunctions extending further into the boundary layer and the profiles becoming more stretched out as roughness is increased. The viscous dissipation term D is dominated by the term $\sigma_{32}\partial\hat{v}/\partial z$ so that $D \approx -(2/Re) \int |\partial\hat{v}/\partial z|^2 dz$. The broadening of the v velocity profile for the Type II mode has the

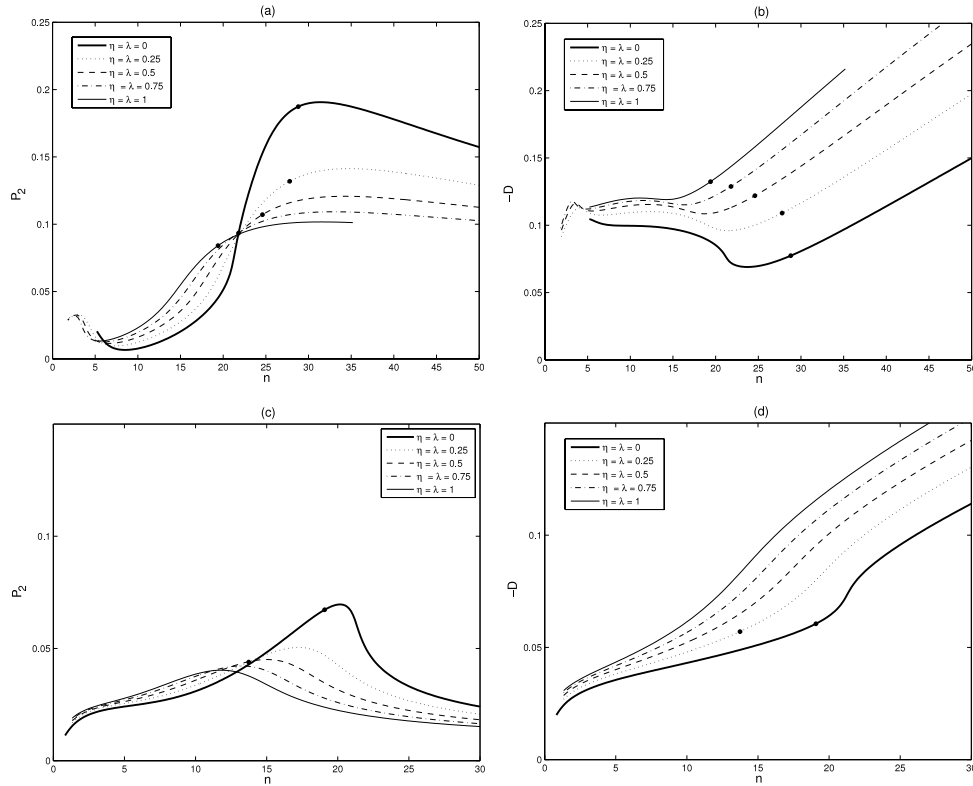


FIG. 9. Energy balance at $Re = 400$ for isotropic roughness. (a) Variation in Type I energy production term P_2 with n , (b) variation in Type I viscous dissipation $-D$ with n , (c) variation in Type II energy production term P_2 with n , and (d) variation in Type II viscous dissipation $-D$ with n . Dots correspond to the locations of maximum amplification in Figure 6.

effect of decreasing D . The effect of roughness on the distribution for D is less significant for the Type I mode.

In summary, the Type II disturbances generally extend further into the boundary layer than the Type I disturbances. The further stretching of the disturbance profile as roughness is increased, together with the slight thickening of the boundary layer, would appear to contribute to the augmentation of the Type II mode under concentric-groove anisotropic roughness.

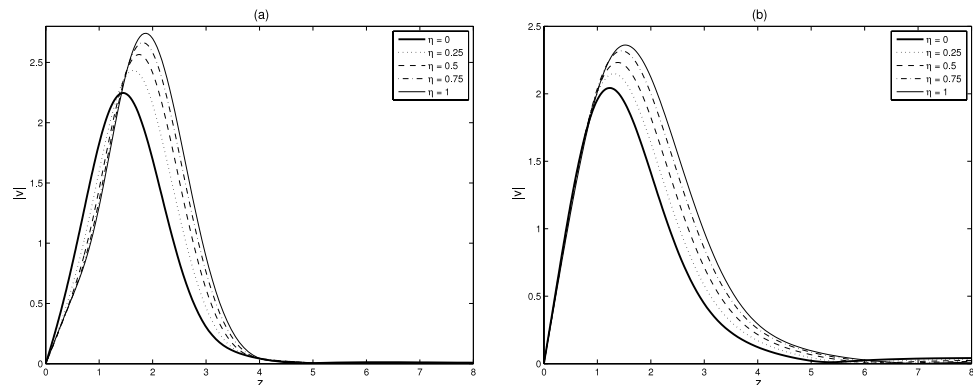


FIG. 10. Profiles for azimuthal perturbation velocity for a concentrically grooved disk at $Re = 400$. (a) Type I eigenmode with $n = 28$ and (b) Type II eigenmode with $n = 8$.

V. TRAVELLING MODES AND ABSOLUTE INSTABILITY

The main focus of this study has been on stationary disturbances, as these are known to be naturally excited by roughnesses on the disk surface. However, non-stationary modes (i.e., those where $\gamma \neq 0$) can also exist, and some have lower critical Re and higher growth rates than the stationary modes. Corke and co-workers^{18,28,29} have shown that non-stationary modes can be important in the transition process over smooth disks, but these tend not to be naturally excited where roughnesses are present. In order to safely predict a stabilization of the boundary layer by surface roughness though, some calculations for travelling modes are included.

Disturbances where $\gamma < 0$ correspond to those travelling inwards on the disk, and those with $\gamma > 0$ correspond to outward-travelling disturbances. Critical Reynolds numbers for the Type II disturbances tend to be lower than for the Type I mode as the frequency increases and some travelling Type I modes have higher growth rates than their stationary counterparts. Since isotropic roughness was found to have a stabilizing effect on both Type I and Type II stationary modes, a single isotropic roughness case ($\lambda = \eta = 0.5$) was chosen to consider the effects of roughness on travelling modes. Neutral curves have been calculated for a range of frequencies and compared to the smooth disk in Figure 11. These show that the effect of roughness remains quite strongly stabilizing for the travelling modes. For the negative frequency chosen ($\gamma = -0.008$), where there is no Type II lobe, this level of isotropic roughness is found to increase the critical Re and also reduce the width of the unstable region. For the positive frequencies chosen ($\gamma = 0.008$ and 0.024), the Type II lobe is significant, but isotropic roughness is found to diminish this region of instability, as well as the Type I region, in a similar way to that observed for the stationary modes. These results allow us to be confident in our conclusions about the stabilizing effects of roughness on the convective instabilities within the boundary layer.

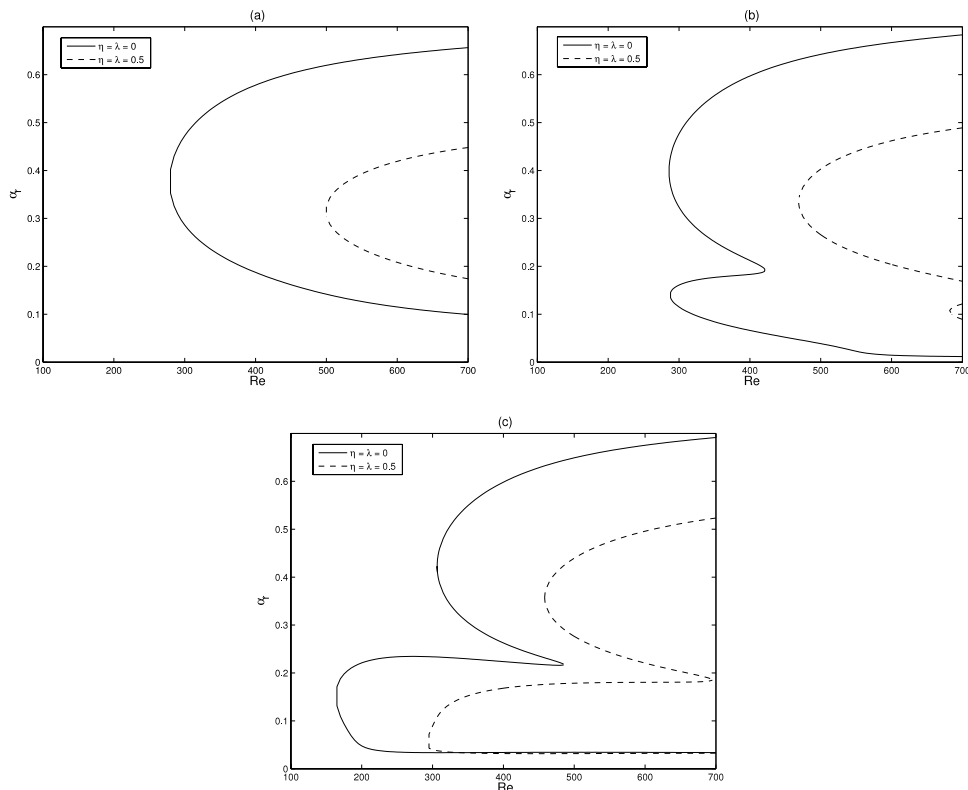


FIG. 11. Effect of isotropic roughness on the neutral curves for travelling modes. (a) $\gamma = -0.008$, (b) $\gamma = 0.008$, and (c) $\gamma = 0.024$.

Another linear eigenmode (Type III) exists in the rotating-disk boundary layer³⁰ which can coalesce with a travelling Type I cross-flow vortex to generate a local absolute instability.¹⁷ This also needs to be considered if inferences about delaying the onset of transition are to be made. The effect of roughness on the growth rate of convective instabilities results in a reduction in their amplification as they propagate downstream. In the case of absolute instability, however, only the suppression of its onset would be beneficial. A significant effect, though, is that if one of the coalescing modes is suppressed, this will at least have the effect of delaying the onset of absolute instability to higher Re . The use of compliant walls to suppress both convective and absolute instabilities in the rotating-disk boundary layer closely parallels this study, and in the compliant wall case³¹ it was found that the stabilizing effect of wall compliance on the Type I mode was indeed effective in delaying the coalescence of the Type I and III modes, thus suppressing the onset of absolute instability. The effects of surface roughness on the absolute instability are the focus of a separate study, but preliminary results have shown that roughness can act in the same way as wall compliance and restrict the onset of absolute instability to significantly higher Re compared to the smooth disk.

VI. SUMMARY AND CONCLUSION

We have summarized and discussed the results of a theoretical study investigating the effects of anisotropic and isotropic surface roughness on the convective stability of stationary disturbances in the boundary-layer flow over a rotating disk. Our theoretical analysis was based on the partial-slip approach for modelling the steady boundary-layer flow over a rough rotating disk. This models roughness by a modification of the no-slip conditions. Our results yield qualitatively consistent results for the three steady-flow velocity components of the rotating-disk boundary layer for increasing roughness levels. Similarly, the subsequent linear stability analysis based on the steady-flow profiles obtained reveals that both anisotropic and isotropic roughness result in a stabilization of the Type I instability mode of the rotating-disk boundary layer, and in the case of anisotropic roughness with concentric grooves a significant destabilization of the Type II mode. These results suggest that a delay in the onset of laminar-turbulent transition may be possible if transition remained via the convective Type I instability route. Our results show that small roughness levels effectively give rise to a perturbation to the smooth-disk mean flow, with the perturbation to the steady flow greatest close to the wall, and this gives rise to a subsequent perturbation to the stability results for the smooth disk.

The results obtained from our linear stability analysis were thereafter reconfirmed by an energy balance calculation. The energy analysis has revealed that for both the Type I and Type II instability modes, the main contributors to the energy balance of the system are the competing mechanisms of energy production by the Reynolds stresses and conventional viscous dissipation. For the Type I mode, all types of roughness considered reduced the maximum amplification rate. At the points of maximum amplification, reduction in energy production by the Reynolds stresses was found to be the main stabilizing mechanism. Calculations suggest that the destabilization of the Type II mode by anisotropic, concentric-groove, roughness results from a reduction in the viscous dissipation. This effect is reversed by radial grooves and isotropic roughness.

The existence of travelling modes and the occurrence of absolute instability are also addressed. The effects of roughness on travelling modes follow the results for stationary modes, in that isotropic roughness is able to increase the critical Re and reduce the amplitudes of both the Type I and II modes. Preliminary results also point to roughness resulting in a significant rise in the Re at which absolute instability arises.

Zoueshtiagh *et al.*²¹ documented a short set of experimental data for velocity profiles over quartz-grain roughened disks. Their results appear to display some qualitative similarities with the data reported here in Figures 1 and 2. However, we believe that a comparison between the data of Zoueshtiagh *et al.*²¹ and the results presented here is not justified for several reasons. The two main reasons being that, first, the roughness considered in the present study is very different compared to the random quartz-grain roughness in Zoueshtiagh *et al.*²¹ Second, the facility of Zoueshtiagh

*et al.*²¹ incorporated a lid covering the disk (see their Fig. 1). The measurements of Colley *et al.*,¹⁰ for flow over smooth disks, have verified that this substantially modifies the boundary conditions in comparison to a disk spinning in an infinite domain. They commented, for instance, on residual motion in the flow above their disks (see Ref. 10, p. 5, left column). Due to this, we have currently begun to computationally investigate the effects of the boundary conditions on the global laminar-flow structure over the disk in order to hopefully become able to distinguish them from the effects due to roughness in future studies. To date there exist no experimental data suitable for a comparison with the theoretical results presented here. In the long term, we plan to conduct a study to acquire such data, as we believe our results show that a full experimental investigation would be a worthy undertaking.

If further theoretical and experimental research into more general forms of roughness can corroborate our results for the isotropic roughness approach used here, then it would point a possible way forward for exploiting the beneficial stabilizing effects of roughness on the Type I mode in future drag reduction techniques, for boundary layers with a cross-flow component. The main results obtained here for general isotropic roughness suggest that there could be practical implications for the development of new roughness-based drag reduction techniques for fully three-dimensional boundary layers. The challenge would be to translate the general form of roughness suggested by the partial-slip parameters into realizable and measurable roughness distributions. The aim would be to design roughness to ensure that the beneficial, stabilizing nature of the effects of roughness on the Type I mode is maximized, whilst avoiding any possible detrimental energy production by Reynolds stresses for the Type II mode.

- ¹ L. Sirovich and S. Karlsson, "Turbulent drag reduction by passive mechanisms," *Nature* **388**, 753–755 (1997).
- ² P. Carpenter, "The right sort of roughness," *Nature* **388**, 713–714 (1997).
- ³ K. S. Choi, "The rough with the smooth," *Nature* **440**, 754 (2006).
- ⁴ J. M. Owen and R. H. Rogers, *Flow and Heat Transfer in Rotating Disc Systems, Vol. I: Rotor-Stator Systems* (Research Studies, Taunton, Somerset, UK, 1989).
- ⁵ H. Schlichting and K. Gersten, *Boundary-Layer Theory*, 8th ed. (Springer, 2000).
- ⁶ M. Wimmer, "Viscous flows and instabilities near rotating bodies," *Prog. Aerosp. Sci.* **25**, 43 (1988).
- ⁷ H. L. Reed and W. S. Saric, "Stability of three-dimensional boundary layers," *Annu. Rev. Fluid Mech.* **21**, 235 (1989).
- ⁸ W. S. Saric, H. L. Reed, and E. W. White, "Stability and transition of three-dimensional boundary layers," *Annu. Rev. Fluid Mech.* **35**, 413–440 (2003).
- ⁹ A. J. Colley, P. J. Thomas, P. W. Carpenter, and A. J. Cooper, "An experimental study of boundary-layer transition over a rotating, compliant disk," *Phys. Fluids* **11**, 3340–3352 (1999).
- ¹⁰ A. J. Colley, P. W. Carpenter, P. J. Thomas, R. Ali, and F. Zoueshtiagh, "Experimental verification of the type-II-eigenmode destabilization in the boundary layer over a compliant rotating disk," *Phys. Fluids* **18**, 054107 (2006).
- ¹¹ S. J. Garrett and N. Peake, "The stability and transition of the boundary layer on a rotating sphere," *J. Fluid Mech.* **456**, 199–218 (2002).
- ¹² S. J. Garrett, Z. Hussain, and S. O. Stephen, "The cross-flow instability of the boundary layer on a rotating cone," *J. Fluid Mech.* **622**, 209–232 (2009).
- ¹³ N. Gregory, J. T. Stuart, and W. S. Walker, "On the stability of three-dimensional boundary layers with application to the flow due to a rotating disk," *Philos. Trans. R. Soc., A* **248**, 155–199 (1955).
- ¹⁴ R. Kobayashi, Y. Kohama, and C. Takamada, "Spiral vortices in boundary layer transition regime on a rotating disk," *Acta Mech.* **35**, 71 (1980).
- ¹⁵ T. Theordorsen and A. Regier, "Experiments on drag of revolving disks, cylinders and streamline rods at high speeds," Technical Reports National Advisory Committee for Aeronautics, Report No. 793, Washington DC, USA, 1945.
- ¹⁶ N. H. Smith, "Exploratory investigation of laminar-boundary-layer oscillations on a rotating disk," Technical Reports National Advisory Committee for Aeronautics, Technical Note No. 1227, Washington DC, USA, 1947.
- ¹⁷ R. J. Lingwood, "Absolute instability of the boundary layer on a rotating disk," *J. Fluid Mech.* **299**, 17 (1995).
- ¹⁸ T. C. Corke and K. F. Knasiak, "Stationary travelling cross-flow mode interactions on a rotating disk," *J. Fluid Mech.* **355**, 285 (1998).
- ¹⁹ S. Jarre, P. Le Gal, and M. P. Chauve, "Experimental study of rotating disk flow instability. II. Forced flow," *Phys. Fluids* **11**, 2985 (1996).
- ²⁰ T. C. Corke and E. H. Matlis, "Transition to turbulence in 3-d boundary layers on a rotating disk-triad resonance," *Proceedings of the IUTAM Symposium on One Hundred Years of Boundary Layer Research, Göttingen, Germany*, edited by G. E. A. Meier and K. R. Sreenivasan (Springer, 2004).
- ²¹ F. Zoueshtiagh, R. Ali, A. J. Colley, P. J. Thomas, and P. W. Carpenter, "Laminar-turbulent boundary-layer transition over a rough rotating disk," *Phys. Fluids* **15**, 2441–2444 (2003).
- ²² T. Watanabe, H. M. Warui, and N. Fujisawa, "Effect of distributed roughness on laminar-turbulent transition in the boundary layer over a rotating cone," *Exp. Fluids* **14**, 390 (1993).
- ²³ M. Miklavčič and C. Y. Wang, "The flow due to a rough rotating disk," *Z. Angew. Math. Phys.* **55**, 235–246 (2004).
- ²⁴ M. S. Yoon, J. M. Hyun, and J. S. Park, "Flow and heat transfer over a rotating disk with surface roughness," *Int. J. Heat Fluid Flow* **28**, 262–267 (2007).

- ²⁵ Th. von Kármán, "Über laminare und turbulente Reibung," *J. Appl. Math. Mech.* **1**, 233-252 (1921).
- ²⁶ R. J. Lingwood and S. J. Garrett, "The effects of surface mass flux on the instability of the bek system of rotating boundary-layer flows," *Eur. J. Mech. - B/Fluids* **30**, 299-310 (2011).
- ²⁷ A. J. Cooper and P. W. Carpenter, "The stability of rotating-disc boundary-layer flow over a compliant wall. Part 1. Types I and II instabilities," *J. Fluid Mech.* **350**, 231-259 (1997).
- ²⁸ H. Othman and T. C. Corke, "Experimental investigation of absolute instability of a rotating-disk boundary layer," *J. Fluid Mech.* **565**, 63 (2006).
- ²⁹ T. C. Corke, E. H. Matlis, and H. Othman, "Transition to turbulence in rotating-disk boundary layers-convective and absolute instabilities," *J. Eng. Math.* **57**, 253 (2007).
- ³⁰ L. M. Mack, "The wave pattern produced by point source on a rotating disk," AIAA Paper No. 85-0490, 1985.
- ³¹ A. J. Cooper and P. W. Carpenter, "The stability of rotating-disc boundary-layer flow over a compliant wall. Part 2. Absolute instability," *J. Fluid Mech.* **350**, 261-270 (1997).